Monitoring ground motion with InSAR EO

Best Practice Guide

Milan Lazecký, Michal Podhoranyi, Georg Zitzlsberger

2022

1. Introduction

We introduce the 'best practice guide' to provide a detailed overview for the processing of satellite interferometric radar data for monitoring ground deformation. The document covers the technical aspects of, and solutions for data acquisition, processing, and visualization; the illustrative input data is from the Copernicus Sentinel-1 satellite mission.

In recent decades, Earth Observation technology, known as Interferometric Synthetic Aperture Radar (InSAR), has developed to the point of achieving the status of full operability, though the use and interpretation of results still requires expert scrutiny. The basic premise follows: specific satellites with an on-board radar system allow active imagery, that is the observed reflection of electromagnetic waves from the surface (through the atmosphere) which can be compared to the original signal, allowing the measurement of both the strength of the reflected signal (amplitude) and the relative delay (phase). As the carrier signal wavelength is known, the phase measurement can be translated to metric units.

A combination of phase measurements from approximately the same location over two satellite passes gives two measurements separated in time, and is the main basis of so-called repeat-pass InSAR, which yields information about relative change over the time period between the satellite passes; the technique can therefore be used to measure the displacement of observed objects (surfaces) with a sensitivity that is proportional to the carrier wavelength. In practice, InSAR is applied to measure the temporal evolution of terrain deformation and displacement of civil infrastructure. Current SAR satellites operate with various parameters. They can allow for high pixel resolution (below 1 m for enhanced spotlight modes) and for high temporal resolution (up to several hours revisit time), and they can make observations using a shorter wavelength to achieve submillimetre accuracy or with a longer wavelength to penetrate through dense vegetation, etc.

In this work, we focus on data from the Copernicus Sentinel-1 SAR satellite system, which observes with a moderate spatial and temporal resolution globally, with data being distributed with an open access policy. As an example, Fig. 1 shows the result of a Persistent Scatterers multitemporal InSAR technique applied on Sentinel-1 to extract vertical displacements of stably backscattering pixels (often urban areas with little vegetation) over the entirety of the Czech Republic by an open source set of processing routines developed at IT4Innovations as the IT4S1 system. The technique is known to deliver measurements of especially vertical displacements with a precision greater than 1 mm/year. This document will further assess the topic in relation to the case study area (terrain deformation in various parts of the Czech Republic), and the system description will also use the Czech Republic as area of interest.

The InSAR capabilities of Sentinel-1 are recognized by various consortia for practical applications from large-scale monitoring in the field of volcanology and tectonics (COMET LiCSAR System, https://comet.nerc.ac.uk/comet-lics-portal) down to the publicly available European-wide high resolution time series products of EGMS (https://egms.land.copernicus.eu).

Although the main scope is InSAR, we have prepared the guide to allow extension to other techniques, such as spectral diversity interferometry for precise extraction of N-S motion, or potentially polarimetric SAR analysis, which is useful in other fields such as land cover identification, oil spill or flood detection etc., though it is not yet broadly applied.

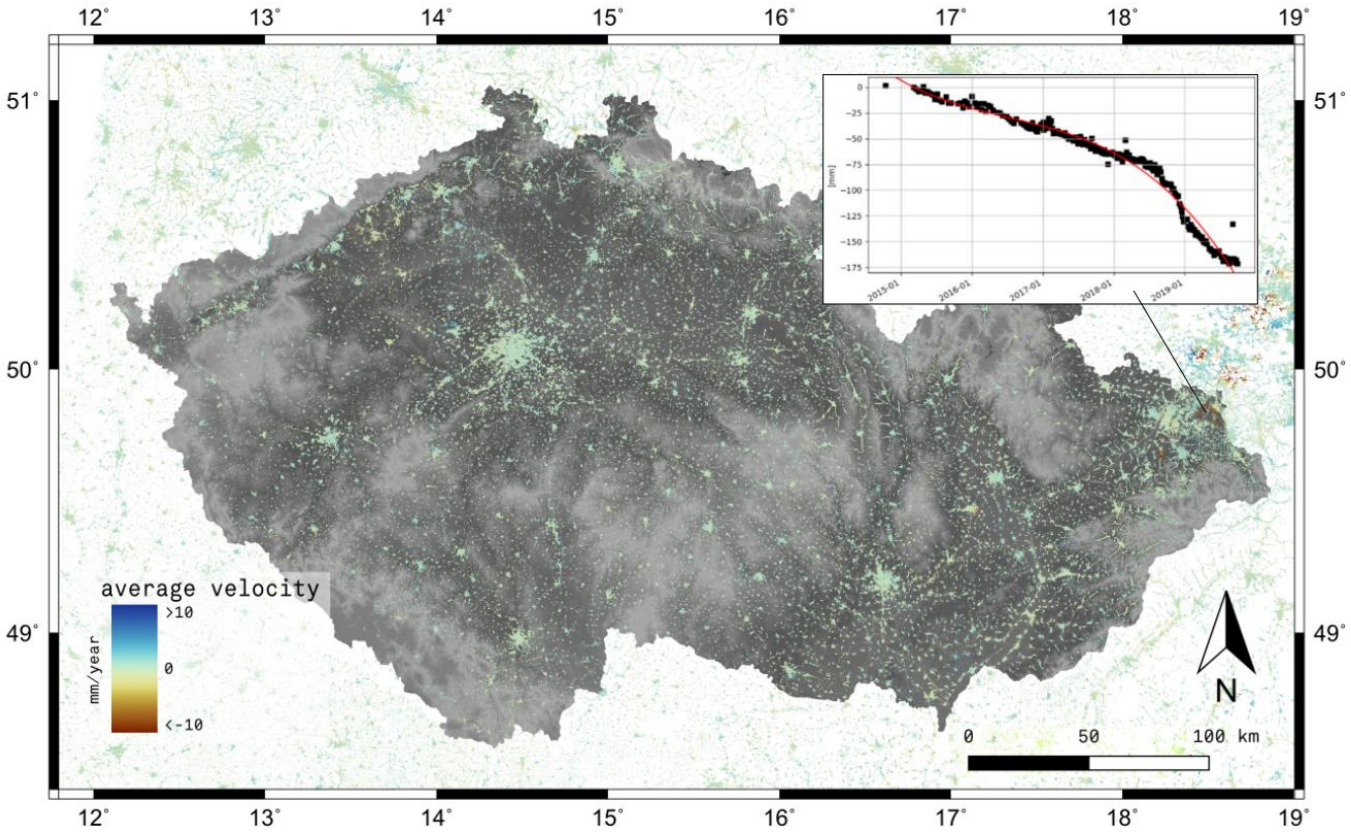

Figure 1. Global output of Persistent Scatterers deformation velocity estimates from Sentinel-1 InSAR over the Czech Republic (downsampled to 100 m). Each coloured pixel in the visualized datacube contains time series information (deformation measurements in millimetres).

2. Data preparation and download

The first and foremost task to perform is to prepare existing Sentinel-1 data, putting it into a form that is ready for interferometric (InSAR) analysis, as this is the main target for detection, measuring, or systematic monitoring of terrain deformation and displacement of infrastructure.

2.1. Acquisition of Sentinel-1 and support data

The Copernicus Sentinel-1 Synthetic Aperture Radar (SAR) satellite constellation has offered medium resolution radar imagery of the European continent every 12 days since October 2014 and every 6 days since autumn 2016. It covers the entire Czech Republic from 9 different orbital tracks (see Fig. 2) and acquires data that are processed and disseminated into zip-compressed single look complex (SLC) data with an annual increment of approx. 6 TB. The data load decreased after the malfunction of Sentinel-1B in December 2021 (the current revisit time has returned to 12 days).

The Sentinel-1 data can be acquired from various sources, yet the primary mirror is a Copernicus Open Access Hub platform: https://scihub.copernicus.eu. Various national initiatives exist, mirroring the data hub, for

example, all SLC files covering the Czech Republic are available at the Czech Copernicus Collaborative Segment (CollGS) maintained by the CESNET organisation: https://collgs.czechspaceportal.cz. Our IT4S1 platform contains procedures for automatized identification and download of the SLC files directly from those sources. Additionally, there are other open source tools that exist for this task, including other data mirrors, such as Alaska Satellite Facility (ASF).

Other data, which support accurate alignment of the SLC imagery including auxiliary calibration files and satellite orbit ephemeris. These are available from the Sentinel-1 Mission Performance Center at https://sar-mpc.eu, and the Copernicus Sentinels POD Data Hub at https://scihub.copernicus.eu/gnss, respectively. Note the highly recommended Precise Orbit Determination (POD) ephemeris are available 21 days after the Sentinel-1 data acquisition. Our IT4S1 platform contains procedures for automatized identification and download of those files.

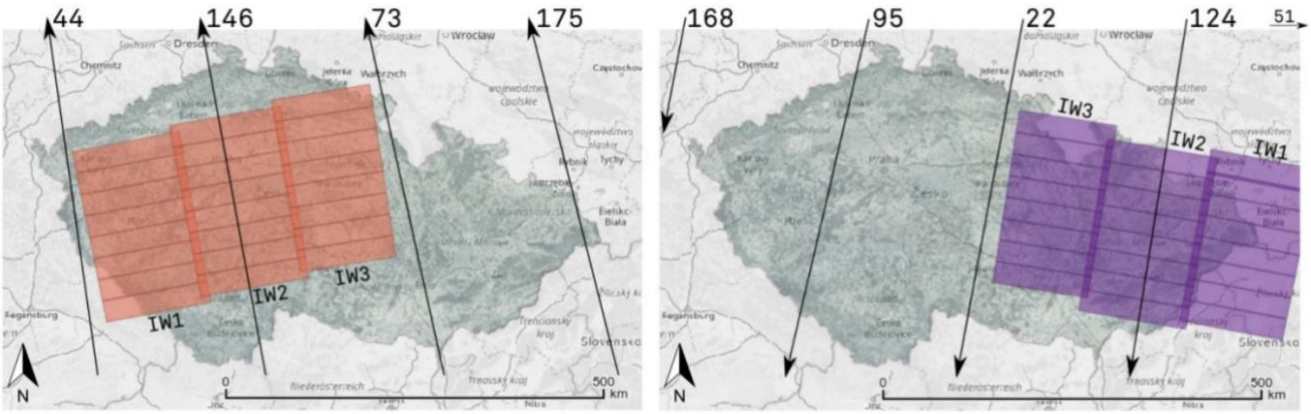

Figure 2. Coverage of the Czech Republic by Sentinel-1 data acquired from a) 4 ascending orbital tracks and b) 5 descending orbital tracks. The filled rectangles map footprints of Sentinel-1 bursts taken from three interferometric wide (IW) swaths, numbered by distance from the satellite as IW1, IW2, and IW3; the footprints are related to data distributed in one zip file.

2.2. Distributed preprocessing

As a reaction to increased demands on data storage and computing resources in the Big Data era, the system IT4S1 has been developed. It establishes a specific workflow for processing data from the Sentinel-1 satellite system, primarily based on open-source tools ISCE2 [1] and solutions developed as part of the open-source LiCSAR system [2].

The core part of the IT4S1 system architecture is a specific method for preprocessing SLC data into the form of a precisely aligned series of images where the coregistration precision is at the level of 0.001 pixels. This is achievable by using interferometric phase information through advanced algorithms, such as the extraction of the enhanced spectral diversity component [3], with an additional approach for removing the phase induced by static topography directly from the SLC data [4]; the resulting new products are directly InSAR-analysis ready, and we call them SLC-C products.

IT4S1 routines connect storage centres of Sentinel-1 SLC data (at CollGS) and final processed SLC-C data. The metadata database system (a metadata base) and the SLC preprocessor are on two separate servers. The metadata database is derived from the LiCSAR LiCSInfo solution, where we simplify the database to only four tables: files, bursts, files2bursts, and bursts2geom. Using the LiCSAR script arch2DB.py, it is possible to read

metadata inside the input SLC zip file to extract information about bursts inside the file, and store it in corresponding tables for further use.

An HPC facility is used for the main SLC-C processing (and later for their InSAR processing); a simplified diagram is shown in Figure 3.

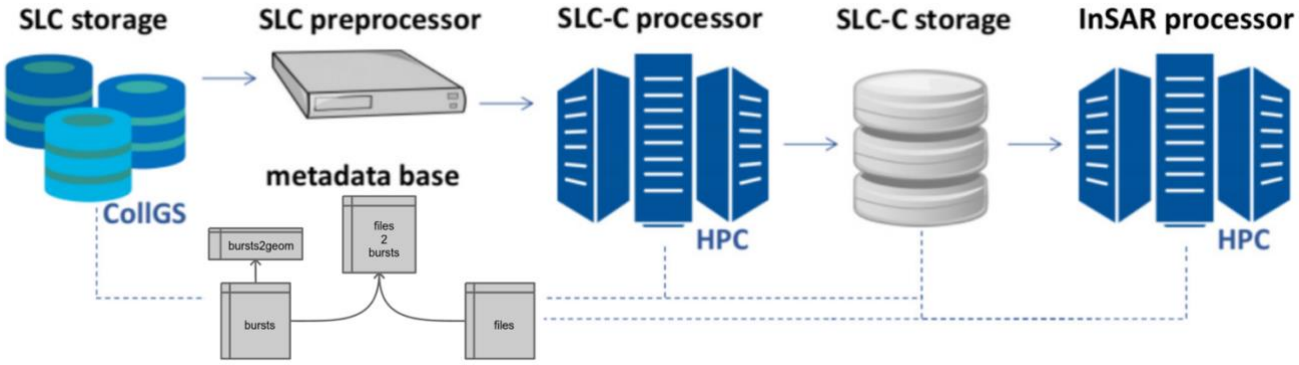

Figure 3. Simple diagram of the IT4S1 architecture for mapping SLC data into metadata database tables and preprocessing them into SLC-C products that can be further used to generate interferometric outputs (e.g. InSAR time series).

After the ingestion of a new Sentinel-1 SLC acquisition to CollGS, a metadata database system solution transferred from LiCSAR [2] ensures the proper identification of its bursts, including information about their geographic coverage. When activated, the SLC preprocessor loads the SLC data with the latest available ephemeris data and splits it into bursts. The SLC preprocessor uses current calibration auxiliary data for Sentinel-1 satellites and the latest ephemeris data for further usage. The high quality Precise Orbit Determination (POD) ephemeris are available 21 days after Sentinel-1 data acquisition, however ISCE processing routines allow a lower-quality on-board ephemeris with no significant loss of performance in further steps. The routines of the ISCE [1] open-source InSAR processing package are run at the SLC preprocessor server and the preprocessed burst SLC images are uploaded to the SLC-C processor (an IT4Innovations HPC facility).

At the SLC-C processor HPC facility, a custom solution prepares coherent burst combinations in order to perform ESD computation and correction. The processing performed is distributed per burst unit. A chronologically preceding set of compatible SLC-C burst images (already existing in the framework of the same relative orbit track) are linked to the processing chain as “primary” burst images. The newly arrived SLC image is recognised as a “secondary” image. The interferometric combinations between both primary and secondary bursts are extremely coherent due to the short temporal revisit time of Sentinel-1, and are therefore highly applicable in ESD computation.

Algorithms of ISCE are applied, performing the preprocessing of secondary bursts until the stage of generating range fine offset fields for every secondary burst. The fine offset field grids contain an estimated non-displacement phase due to the stereoscopic effect of topography observed from two slightly different satellite positions at both the primary and secondary bursts. In order to simulate this topographic phase, we apply an SRTM 1 arc-second digital elevation model (DEM) [5] to form a height-per-pixel image fitting the primary bursts during the initial step. The range offset fields are removed from the secondary bursts, and these are saved into an SLC-C storage for further use. Such produced SLC-C data are ready for direct generation of a topography-free interferogram [4] with a simple operation of complex conjugation

The coregistration process of a new acquisition A follows the original procedure as implemented by ISCE topsApp.py script [6], until the fineresamp step. The existing geom data (containing lookup tables of 3-D geographic coordinates towards primary SLC data) are linked, rather than regenerated. Where there are other existing SLC-C files in the database, a check is performed, and the burst SLC-C images of an acquisition B closest

in time to the acquisition A data are linked as secondary reference data. The primary reference SLC data would be used to support the coregistration step by an amplitude cross-correlation, while the ESD estimation is performed towards the secondary reference data, not directly to the SLC data of the primary acquisition. As tested in [4] and shown in the results later on, we did not identify significant bias in full resolution interferometric combinations caused by this cascade approach over the mid-European region, as the coregistration accuracy is kept high, to the level of 0.001 pixels [7].

The key outputs of the ISCE topsApp.py coregistration approach, used as the basis for SLC-C generation, are range and azimuth fine-offset files, correcting for subpixel misregistration in the range and azimuth directions. These include both DEM-based height correction, ESD-based correction, and other refinements [6]. After the range offsets (that directly affect the measured phase and contain the estimated topography phase) are removed from the resampled burst images [1], the final coregistered phase-corrected product is generated for the given temporal epoch. We refer to such products as SLC-C, and store them in the final product data storage.

The SLC-C images can be directly transformed into georeferenced imagery using a geocoding look-up table (generated by ISCE2) and then ingested into a datacube for further processing, as the final InSAR analysis ready data; for such purposes, we apply a set of xarray-led python libraries, and further distribute the datacube as a multidimensional NetCDF file.

2.3. Systematic data storage

The Czech analysis ready data are stored as burst units that are an area typically 20x80 km in approximately latitude x longitude directions, in a resolution of approximately 14x3 m (ground range). External grids per burst containing coordinates can be used to transform the data into radar coordinates as per the WGS-84 geographic system. The data allow direct processing using interferometric methods (InSAR), as they are already precisely coregistered, including spectral diversity correction and removal of topography-correlated phase [8].

The LiCSAR-based metadata database runs on a dedicated MySQL server, and the generated SLC-C data are permanently stored on a dedicated shared disk, both within the CESNET infrastructure. CESNET's MetaCentrum computing infrastructure was used for an initial preparation of SLC data prior to their main processing towards SLC-C (at IT4Innovations HPC).

In the first step, a systematic data storage environment is established, aiming for the data storage structure: RELORB/SWATH/BURST_TANX/YEAR, where RELORB is a relative orbital track number of Sentinel-1 satellites, SWATH is a number from 1–3 identifying one of the three Sentinel-1 swaths, and BURST_TANX is a burst identifier based on a naming convention established by the LiCSInfo approach of the LiCSAR system [2]. In order to avoid having a large number of files in the BURST_TANX folder, we sort them into the subfolder YEAR (year of acquisition date). The names of the SLCC files are in the form of YYYYMMDD.slc (e.g., 20200201.slc for an SLCC image from the 1st of February 2020).

We establish a base dataset for each RELORB/SWATH. Here, we manually select the primary SLC image, with the main condition of having a full burst coverage across the whole region of interest (across the Czech Republic in this case). The initial processing is performed by the original ISCE approach. Based on the acquisition metadata and automatically downloaded SRTM DEM, ISCE generates files containing latitude, longitude, height and line of sight (LOS) angle values for every pixel in the reference SLC image. These files are modified and stored per burst, i.e., under the BURST_TANX subfolder, in a geom folder.

Sentinel-1 data covers the entire Czech Republic over 9 tracks, yielding approximately 180 new images per month. One image contains 24 bursts (8 bursts per 3 swath units), covering an approximately 90 × 20 km area each, with an LOS direction pixel spacing of approximately 3 × 14 m [9], and is distributed in files of approximately 4.5 GB in their compressed form, i.e., approx. 200 MB/burst in the compressed form and around

550 MB uncompressed (including both copolarised and cross-polarised images). For InSAR, only copolarised images are needed. We stored our generated SLCC burst images compressed to approximately 200 MB/burst.

In October 2017, 3,580 unique Sentinel-1 SLC zip files covering the Czech Republic were stored in CollGS (~15.7 TB), while in December 2020 the number was 7740 SLC files (~34 TB). The full dataset of SLC-C images consisted of ~8 TB in October 2017, and it approached 20 TB in December 2020, with the monthly data size increment for Czech bursts being ~360 GB/month before the failure of the Sentinel-1B satellite in December 2021, with it now being ~180 GB/month.

2.4. Inclusion of other data

The current storage allows identification of burst cubes with standard metadata; this can be extended for further satellite missions, such as BIOMASS (2023), NISAR (2024), or other data that is classified as open access. However, special care should be taken for effective systematisation of the precisely coregistered dataset, as the data takes would not be compatible with the established burst units of Sentinel-1. A custom solution for making datacube tiles in an organised manner with a view to doing cross-platform analyses can be recommended here. If the sub-millimetre precision is not required (e.g. Persistent Scatterers or other technique that would exploit the signal of objects with a stable and dominant reflection), one may multilook such data from other SAR missions and georeference them to the final set of datacube tiles, or use an existing system, such as the rasdaman raster geodatabase.

Later on, the look up tables created by ISCE2 for the precise coregistration can also be applied to another polarisation band if it exists within the same data take. This way the InSAR data cubes can be directly augmented to allow polarimetric analyses.

3. Interferometric analysis

A topography-free interferogram can be formed simply by a complex conjugation between any two SLC-C files. The generated interferogram would be affected by various signal sources, including noise. To measure the quality of the interferometric signal, IT4S1 can calculate coherence maps.

We have formed coherence matrices from 15,932 interferometric combinations of a selected burst (ID 95_1_21244) from the period between February 2015 to May 2019 (plotted in Figure 4). The coherence matrices show the median coherence over small areas (~1000 pixels) representing two different types of scattering classes: urban and agricultural land types. The matrices can be used as a quality measure, demonstrating that the interferometric signal is also coherent in combinations of SLC-C files in very distant temporal baselines, as in the case of urban areas (Figure 4a). The effect of signal decorrelation related probably to the presence of snow in winter months can be observed as drops of coherence. The selected agricultural area decorrelates especially in summer months (Figure 4b), as expected.

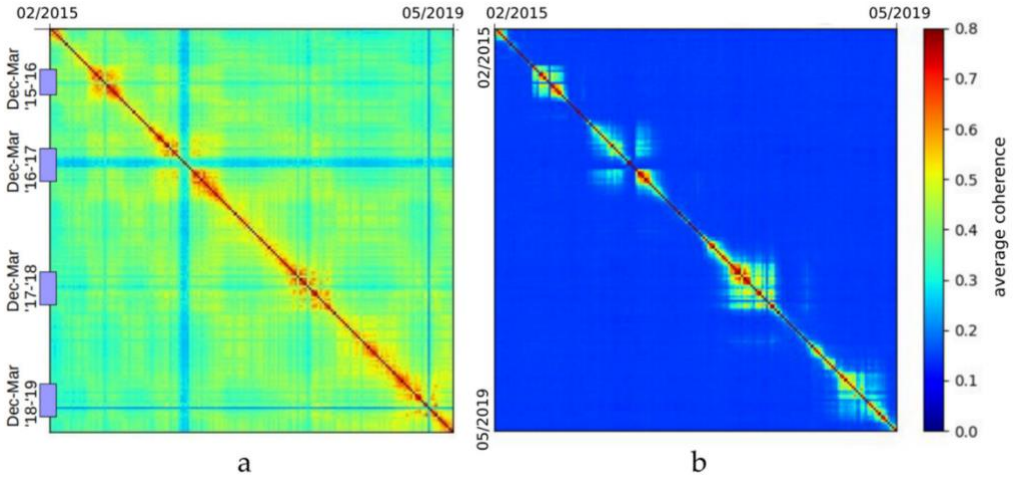

Figure 4. Interferometric coherence matrices of burst ID 95_1_21244 (February 2015—May 2019) over (a) an urban area and (b) an agricultural area.

3.1. Generation of base interferometric products

As mentioned before, starting from InSAR ARD burst units reduces the InSAR processing chain significantly. The input for generating an interferogram (followed eventually by spatial filtering and unwrapping) is two burst grids that can be automatically clipped based on user input parameters. In the case of highest resolution and full bursts, the two grids have a typical size of 2x180 MB.

Without the ARD, the processing chain would consist of downloading two SLC files per 4.7 GB and performing the computationally heavy process of coregistration based on intensity cross-correlation and spectral diversity estimation within burst overlaps (an operation that would fail if the acquisitions are temporally distant, i.e. if the signal is decorrelated). Datacube generation systematically processes SLCs subsequently in time, therefore the chance of spectral diversity failure is low and the estimate is precise.

3.2. Estimation of non-deformation signal and phase unwrapping

As the interferograms contain other signals than those only due to terrain deformation, there are approaches that exist to map and improve their quality, starting from adaptive spatial filtering [10], to the use of existing models, e.g. DEM for residual topographic signal and coarse estimate of height-related tropospheric signal, orbital ramps from precise ephemerides, models of tropospheric and/or ionospheric delay, and other third party data to decrease phase gradients in interferograms. As the interferograms are phase-wrapped, i.e. measurement is within the boundaries of the wavelength of the SAR intstrument carrier signal, removal of noise is necessary to increase the probability of correct phase unwrapping. There are various techniques that exist for such operations. IT4S1 uses a standard spatial filtering method and the open-source unwrapper ‘snaphu’ [11] if needed prior to performing time series inversion. It can be recommended to further implement advanced routines for decreasing the phase bias found in interferometric loop closure triplets after multilook operation [12], or directly modelling it to novel applications, such as for the monitoring of landcover dynamics (e.g. annual changes of vegetation seasonality, growth or long term soil moisture changes) [13].

The main advantage of using time series inversion to assess interferometric combinations is the possibility to further reduce the non-deformation signal by mathematical modelling of the atmospheric phase screen [14], making corrections using the correlation of phase data with temperature values (e.g. thermal dilation of bridges [15], seasonality in time series) or water levels if the object to observe is a dam construction [16] etc.

3.3. Time series inversion

Perhaps with the exception of SARPROZ software that analyses coregistered SAR data stacks directly to reach interferometric outputs, all standard InSAR approaches analyse products called interferograms, generated by a complex multiplication and further post-processing of pairs of coregistered images. With the existing InSAR ARD, the process of generating an interferogram is a simple and fast operation on two images (temporal epochs) of a burst datacube. Depending on the method used for time series inversion, e.g. Persistent Scatterers (PS) [17], Small Baselines (SB) [18], NSBAS [19], the phase linking technique [13] etc., our routines prepare a network of interferometric pairs, and generate their interferometric products (including a coherence map) and additional products (e.g. amplitude stability index) that are then used as an input for the time series inversion or other analyses (e.g. machine learning detection of anomalies).

Related to the time series being the most important output of InSAR analysis, Fig. 5 demonstrates the results from three different popular algorithms over CSM Mine, using STAMPS [14] and LiCSBAS [20] open-source software. While PS connects all temporal epochs to one reference epoch, and analyses only points that are stably backscattering through time (thus their phase is highly coherent in time and can be assessed reliably), the SB-based techniques combine temporal epochs in pairs that are close to each other in time to assess the spatially coherent phase also of pixels that drop their coherence quickly (e.g. vegetated areas). Such pixels are less reliable but may still contain important information on surface deformation. For the output of NSBAS in Fig. 5, we did not mask pixels based on any of the available measures of quality. Here we include noisy pixels in the final result that might be interpreted as non-deformation signal related to the processes of vegetation growth.

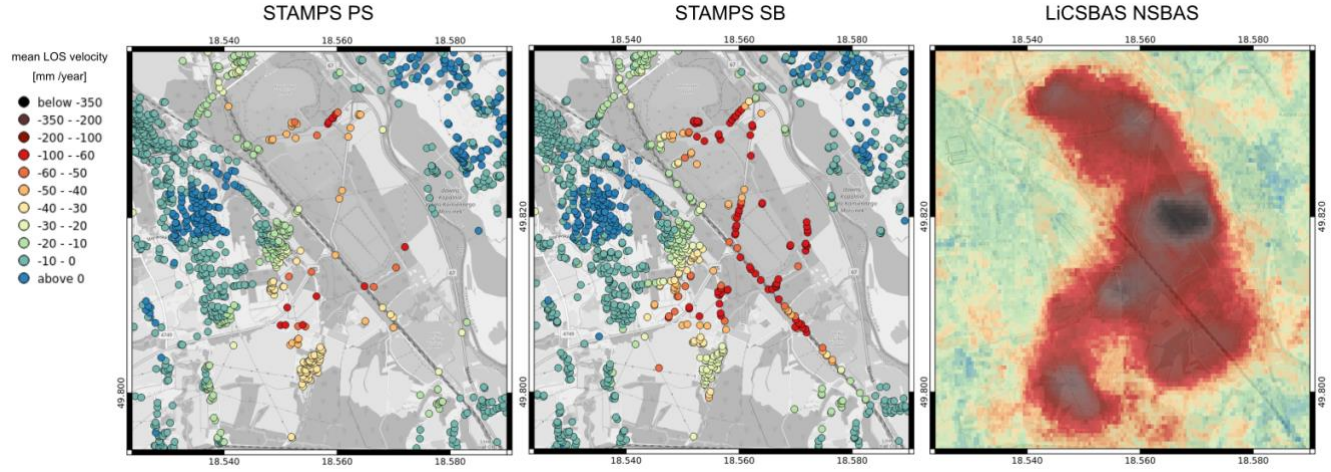

Figure 5. Differences between processing results of the PS, SB, and (non-masked) NSBAS methods over an undermined area (CSM Mine).

The IT4S1 architecture allows the advantageous use of on-demand processing of a selected area of interest (AOI). They script it4s1_process_all.sh takes latitude and longitude as coordinates for the centre point and radius of interest in kilometres, as basic parameters. When connected to a burst metadata database, the script could identify bursts covering the AOI, select overlapping bursts, and generate their interferograms in combinations set up based on the requested processing method. These interferograms are generated in radar coordinates, either within the full burst, or cropped to the selected extents.

As outputs of the requested processing methods (STAMPS PS only by default), the system generates comma-separated text (CSV) files for each burst ID containing computed measures such as a mean velocity rate, temporal coherence, estimated deformation value per image date, and other parameters (e.g., the standard deviation of the estimated velocity). Optional processing parameters include start and end dates, other processing techniques to be applied, and a reference area.

Processing parameters for STAMPS algorithms are scaled automatically in relation to the size of the selected area. An overview of selected parameters and their use is shown in Table 2 of [8], and an explanation of the parameters can be found in [21]. The parameters drive several key components of STAMPS during its selection of pixels to be processed, estimation of non-deformation signal, and the final inversion to the deformation time series. We keep the parameters oriented to indicate deformation on a small to moderate scale (e.g., we remove long wavelength deformation through a deramping over the whole region, using the parameter scla_deramp).

The processing chain starts by clipping the dataset to smaller data patches that are processed in parallel (one patch per processing core). Within each patch, we select pixel candidates based on the amplitude dispersion index (ADI) [14] computed from interferogram magnitude images. Afterwards, we run STAMPS steps [21] 1, 2 (read data and estimate phase noise for them) and 4 (dropping pixels based on their noise standard deviation: weed_standard_dev); step 3 (selection of pixels based on their spatial consistence) is skipped. We report the possibility for the direct use of Octave to run the STAMPS scripts for steps 1–4.

We then merge the patches through STAMPS step 5 (and merge them to a grid of resolution: merge_resample_size). Next, steps 6 (3-D phase unwrapping) and 7 (estimation of a spatially-correlated look angle error, including correction of phase induced through atmosphere) iterate. In total, 6 iterations are performed, refining the error terms to improve the estimation of unwrapped phases (step 6). Almost every iteration includes a specific optimisation to select the input set of interferograms (based on their noise standard deviation, ifg_std, computed using ps_calc_ifg_std), perform atmospheric phase correction, (optionally) carry out 2-D deramping of the overall spatial phase ramp, etc. Finally, a custom approach is used to compute the standard deviation and temporal coherence of the output estimates [4, 22].

Additionally, the data generated for STAMPS processing were optionally used for preprocessing using other algorithms implemented within the system; specifically an octave-based SALSIT PS software [4] and a python-based LiCSBAS software [20] that can be recommended for further use with multilooked InSAR ARD datacubes.

Depending on the number of points to process and the size of the dataset, a typical burst datacube was processed by the STAMPS PS InSAR approach within 24–48 core-hours (in the case of a 100 interferograms dataset, formed in connection to a common primary SLC-C), while it can take 72–96 core-hours for the STAMPS SB InSAR approach (in the case of the same SLC-C dataset, this would consist of 400 interferograms formed by default for the SB approach, combining data in the 4 shortest temporal connections). We report that we experienced an increase of processing time when the MATLAB scripts of STAMPS (steps 1–4) were run through the open-source Octave environment. We did not perform a similar benchmark for LiCSBAS, but it is known to be more effective; on the other hand, interferometric data must be fully unwrapped processing that is resource intensive, depending on unwrapping parameters and strategy [11].

4. Post-processing, analysis, and interpretation of results

Various existing works show examples of well-applicable InSAR post-processing approaches, including machine learning for detection of volcanic activity, LSTM neural networks for identification of landslides or other hazardous signals in time series, finding deviations from long-term geophysical processes (e.g. long-term influence of underground gas holders), and other uses based on both deformation measurements in urban areas (monitoring of vertical displacements of building, bridges etc. a precision below 1 mm/year) and in nature (from detection of slope instabilities to measurements of tectonic plate motion).

As a very simple example, we show the result of annual deformations over a mining area around the CSM Mine, Karvina, the Czech Republic from LiCSBAS processing of InSAR datacubes from all 4 available satellite tracks (in descending and ascending orbital pass) that covered the area. Frome these, we acquired 4 datacubes with time

series covering the period of 2015-2020, differing by satellite line of sight (LOS). We estimated annual velocities from the datacubes and decomposed the measurement vectors from the 4 lines of sight into vertical and horizontal (eastwards) motion components [23]. Afterwards, we extracted isolines and plotted the results together with polygons of mining activity that was performed in the respective year. The overview is shown in Figure 6.

Note that the interferometric signal can be affected by various kinds of noise, and that the quality of outputs of InSAR analysis depend on various factors, including statistical limits such as the size of the input dataset. It is recommended to have a working knowledge of proper interpretation of InSAR signals and to obtain reliable verification and validation data prior to concluding interpretations. There are various examples of world-leading scientific groups, companies, and other institutes using InSAR data as a unique source of critical information, such as detection of volcanic activity prior to eruption, formation of sinkholes, change of deformation velocity over hill slopes or ice sheets, unexpected subsidence signal over buildings etc., yet conclusions established solely from InSAR results are rare.

5. Data visualization

In the current version of IT4S1, the results from MT-InSAR are exported into a comma-delimited text file (CSV) in order to import to a GIS interface. The CSV includes the estimated LOS displacement values per each date, linear velocity estimates, estimates of the residual height of the pixel, geographic coordinates as per the WGS-84 system, temporal coherence, and a standard deviation of the velocity estimate based on [4].

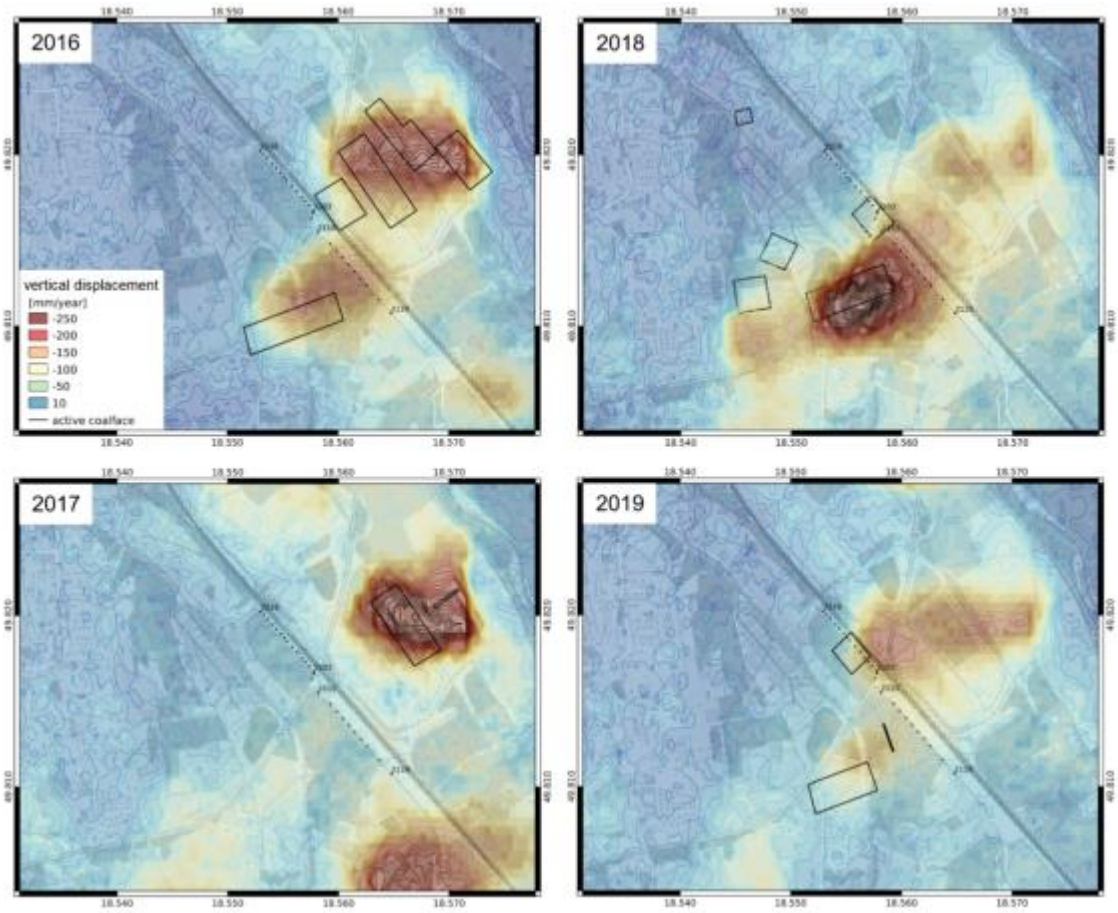

Figure 6. Vertical deformation over the CSM Mine area in annual steps from IT4S1 datacubes processed by LiCSBAS.

Although the Floreon+ system offers a web GIS environment, we kept the current outputs publicly available only in its simplified web map: http://seth4.ics.muni.cz/lazecky contains basic results from STAMPS PS processing over all burst units in the Czech Republic; see Fig. 7, which demonstrates the contents of the webmap. A part of the processing is included in the Floreon+ webmap: https://floreon.eu/mapa.

For the plotting of time series figures for a selected point we currently use a custom giSAR toolbox [24] developed for Quantum GIS, but there are other related plugins that are available, or that could be further developed for QGIS or a python environment.

To follow current trends, we propose the conversion of the complex number binary files in radar coordinates to the final InSAR analysis ready data (InSAR ARD), that is to use existing standard routines to geocode the burst products to the same grid per burst, and be stored as amplitude and phase bands per temporal epoch. We explored possible data storage solutions and found projects like rasdaman to be effective for those purposes, yet the development of a native datacube on top of other existing solutions can also be applied here.

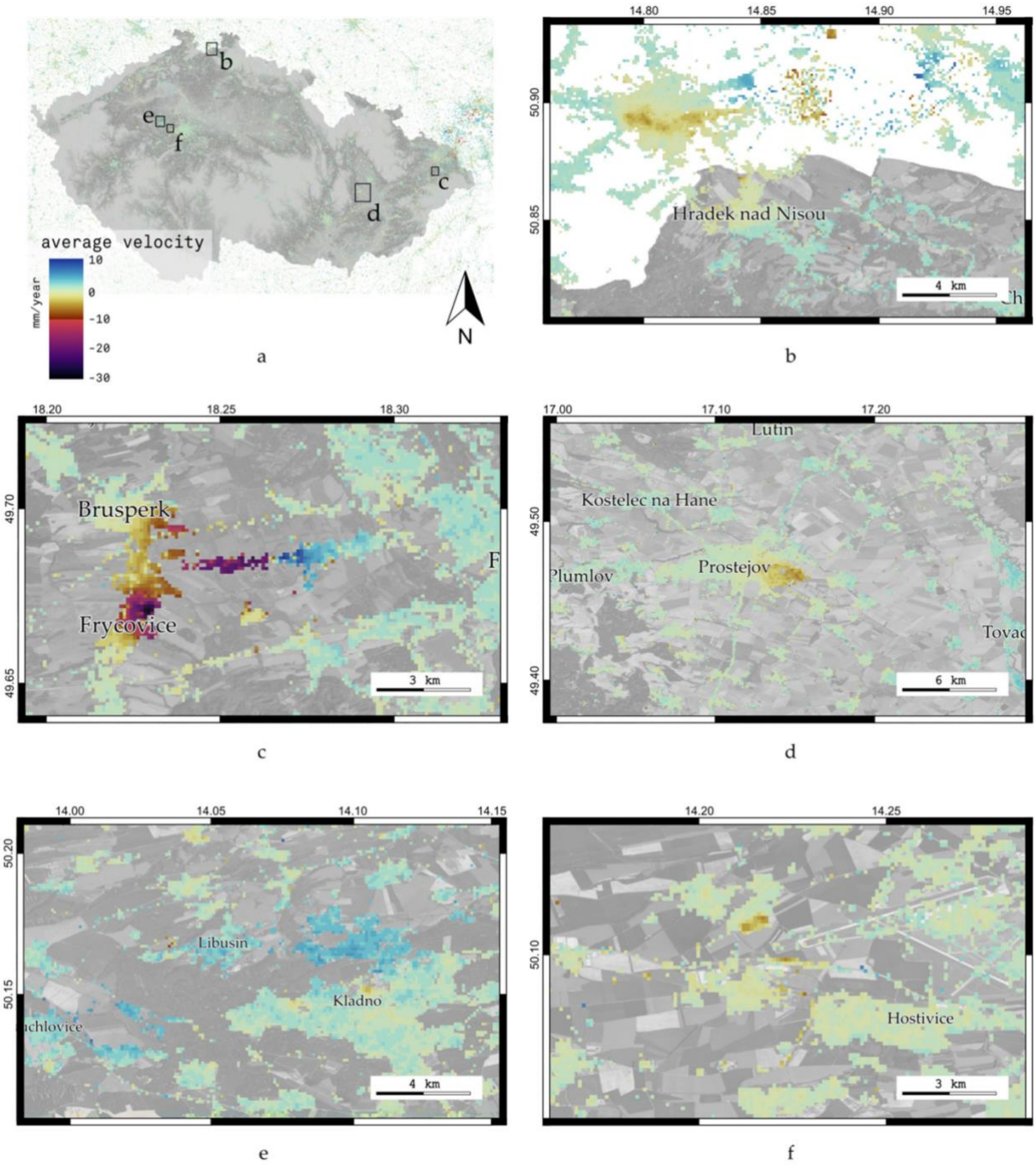

Figure 7. Examples of detected terrain deformations within the full-scale nationwide PS processing (Sentinel-1 data from October 2014–September 2017, processed by STAMPS PS through the IT4S1 system): (a) Map overview localising zoomed-in areas in this figure, (b) subsidence in the surroundings of Turów, (c) subsidence and uplift due to mining activities in the Brusperk area, (d) settlement in the industrial zone of Prostejov, (e) uplift in the surroundings of Kladno, (f) local subsidence near Hostivice.

6. Summary and Conclusion

We present a general guide to assess InSAR data for popular applications in deformation monitoring, which includes monitoring of displacements of urban structures (e.g. bridges, dams, buildings etc.), detection of slope instabilities (signal preceding landslides), larger scale ground motion (volcanic or tectonic deformation), etc. We show basic examples of subsidence across regions in the Czech Republic, as assessed from Sentinel-1 data.

This best practice guide provides a detailed manual for how to measure ground deformation using InSAR techniques, using open-access Copernicus Sentinel-1 Interferometric Wide Swath data, on an example application for the Czech Republic. We present routines implemented through open source software, packaged in the IT4S1 system solution. The system and its results can find application in national geologic, urban planning, forestry or risk management applications, such as, e.g., Floreon+ developed by IT4Innovations to support local risk management [31]. The IT4S1 could be further developed in this framework in the direction of an automatic InSAR-based system that would make it possible to provide an early warning by detecting displacements around critical AOIs based on change analyses in interferometric time series.

References

1. Zebker, H.A.; Hensley, S.; Shanker, P.; Wortham, C. Geodetically Accurate InSAR Data Processor. IEEE Trans. Geosci. Remote Sens. 2010, 48, 4309–4321.

2. Lazecký, M.; Spaans, K.; González, P.J.; Maghsoudi, Y.; Morishita, Y.; Albino, F.; Elliott, J.; Greenall, N.; Hatton, E.; Hooper, A.; et al. LiCSAR: An Automatic InSAR Tool for Measuring and Monitoring Tectonic and Volcanic Activity. Remote Sens. 2020, 12, 2430, doi:10.3390/rs12152430

3. Yague-Martinez, N.; Prats-Iraola, P.; Gonzalez, F.; Brcic, R.; Shau, R.; Geudtner, D.; Eineder, M.; Bamler, R. Interferometric Processing of Sentinel-1 TOPS Data. IEEE Trans. Geos. Remote Sens. 2016, 54, 2220–2234.

4. Lazecky, M.; Hlavacova, I.; Martinovic, J.; Ruiz-Armenteros, A.M. Accuracy of Sentinel-1 interferometry

monitoring system based on topography-free phase images. Procedia Comput. Sci. 2018, 138, 310–317.

5. Farr, T.G.; Rosen, P.A.; Caro, E.; Crippen, R.; Duren, R.; Hensley, S.; Kobrick, M.; Paller, M.; Rodriguez, E.; Roth, L.; et al. The shuttle radar topography mission. Rev. Geophys. 2007, 45, 1–33.

6. ISCE Team, Overview of S1A TOPS Processing with ISCE –topsApp.py. Available online: http://etdedata.gein.noa.gr/ISCE_UNAVCO/topsApp_ISCE_20160418.pdf (accessed on 31 July 2020).

7. Qin, Y.; Perissin, D.; Bai, J. Investigations on the coregistration of Sentinel-1 TOPS with the conventional cross-correlation technique. Remote Sens. 2018, 10, 1405.

8. Lazecký, Milan, Emma Hatton, Pablo J. González, Ivana Hlaváčová, Eva Jiránková, František Dvořák, Zdeněk Šustr, and Jan Martinovič. 2020. "Displacements Monitoring over Czechia by IT4S1 System for Automatised Interferometric Measurements Using Sentinel-1 Data" Remote Sensing 12, no. 18: 2960. doi: 10.3390/rs12182960.

9. Bourbigot, M.; Johnsen, H.; Piantanida, R.; Hajduch, G.; Poullaouec, J. Sentinel-1 Product Definition, Technical Report Ref. S1-RS-MDA-52-7440. Available online: https://sentinel.esa.int/documents/247904/1877131/Sentinel-1-Product-Definition (accessed on 20 February 2020).

10. R. M. Goldstein and C. L. Werner, "Radar interferogram filtering for geophysical applications", Geophys. Res. Lett., vol. 25, no. 21, pp. 4035-4038, Nov. 1998.

11. Chen, C.W.; Zebker, H.A. Phase unwrapping for large SAR interferograms: Statistical segmentation and generalized network models. IEEE Trans. Geosci. Remote Sens. 2002, 40, 1709–1719.

12. De Zan, F., Zonno, M., & López-Dekker, P. (2015). Phase Inconsistencies and Multiple Scattering in SAR Interferometry. IEEE Transactions on Geoscience and Remote Sensing, 53, 6608-6616

13. Ansari, H., Zan, F.D., & Parizzi, A. (2021). Study of Systematic Bias in Measuring Surface Deformation With SAR Interferometry. IEEE Transactions on Geoscience and Remote Sensing, 59, 1285-1301

14. Hooper, A. A multi-temporal InSAR method incorporating both persistent scatterer and small baseline approaches. Geophys. Res. Lett. 2008, 35, L16302, doi:10.1029/2008GL034654.

15. Lazecky, M.; Bakon, M.; Hlavacova, I.; Sousa, J.J.; Real, N.; Perissin, D.; Patricio, G. Bridge Displacements Monitoring using Space-Borne SAR Interferometry. IEEE J. Sel. Top. Appl. Earth Obs. Rem. Sens. (J-STARS) 2016, 10, 205–210.

16. Ruiz-Armenteros, A.M.; Lazecky, M.; Hlavacova, I.; Bakon, M.; Delgado, J.M.; Sousa, J.J.; Lamas-Fernández, F.; Marchamalo, M.; Caro-Cuenca, M.; Papco, J.; et al. Deformation monitoring of dam infrastructures via spaceborne MT-InSAR: The case of La Viñuela (Málaga, southern Spain). Procedia Comput. Sci. 2018, 138, 346–353.

17. Ferretti, A.; Prati, C.; Rocca, F. Nonlinear subsidence rate estimation using Permanent Scatterers in differential SAR interferometry. IEEE Trans. Geos. Remote Sens. 2000, 38, 2202–2212, doi:10.1109/36.868878.

18. Berardino, P.; Fornaro, G.; Lanari, R.; Sansosti, E. A new algorithm for surface deformation monitoring based on small baseline differential SAR interferograms. IEEE Trans. Geosci. Remote Sens. 2002, 40, 2375–2383.

19. Schmidt, D.A.; Bürgmann, R. Time-dependent land uplift and subsidence in the Santa Clara valley, California, from a large interferometric synthetic aperture radar data set. J. Geophys. Res. Solid Earth 2003, 108, 2267, doi:10.1029/2002JB002267.

20. Morishita, Y.; Lazecky, M.; Wright, T.J.; Weiss, J.R.; Elliott, J.R.; Hooper, A. LiCSBAS: An Open-Source InSAR Time Series Analysis Package Integrated with the LiCSAR Automated Sentinel-1 InSAR Processor. Remote Sens. 2020, 12, 424, doi:10.3390/rs12030424.

21. Hooper, A.; Bekaert, D.; Hussain, E.; Spaans, K.; Arikaan, M. StaMPS/MTI Manual. Available online:

https://github.com/dbekaert/StaMPS/blob/master/Manual/StaMPS_Manual

22. Colesanti, C.; Ferretti, A.; Novali, F.; Prati, C.; Rocca, F. SAR Monitoring of Progressive And Seasonal Ground Deformation Using the Permanent Scatterers Technique. IEEE Trans. Geosci. Remote Sens. 2003, 41, 1685–1701.

23. Wright, T.J.; Parsons, B.E.; Lu, Z. Toward mapping surface deformation in three dimensions using InSAR. Geophys. Res. Lett. 2004, 31, 1–5.

24. giSAR (Quantum GIS Toolbox). Available online: https://github.com/espiritocz/giSAR (accessed on 20 February 2020).

25. Overview of NISAR Mission and Airborne L & S SAR. Available online: https://vedas.sac.gov.in/vedas/downloads/ertd/SAR/L_1.pdf (accessed on 25 May 2020).

26. Lazecky, M.; Lhota, S.; Wenglarzyova, P.; Joshi, N. Evaluation of forest loss in Balikpapan Bay in the end of 2015 based on Sentinel-1A polarimetric analysis. In Proceedings of the IGRSM 2018, Kuala Lumpur, Malaysia, 24–25 April 2018.

27. Lazecky, M.; Wadhwa, S.; Mlcousek, M. Simple method for identification of forest windthrows from Sentinel-1 SAR data incorporating PCA. In Proceedings of the CENTERIS SARWatch 2020, Vilamoura, Portugal, 21–23 October 2020.

28. Nielsen, A.A.; Canty, M.J.; Skriver, H.; Conradsen, K. Change detection in multi-temporal dual polarization Sentinel-1 data. In Proceedings of the 2017 IEEE International Geoscience and Remote Sensing Symposium (IGARSS), Fort Worth, TX, USA, 23–28 July 2017.

29. De Luca, C.; Zinno, I.; Manunta, M.; Lanari, R.; Casu, F. Large areas surface deformation analysis through a cloud computing P-SBAS approach for massive processing of DInSAR time series. Remote Sens. Environ. 2017, 202, 3–17.

30. Fattahi, H.; Agram, P.; Simons, M. A network-based enhanced spectral diversity approach for TOPS time-series analysis. IEEE Trans. Geosci. Remote Sens. 2017, 55, 777–786.

31. Podhoranyi, M.; Veteska, P.; Szturcova, D.; Vojacek, L.; Portero, A. A web-based modelling and monitoring system based on coupling environmental models and hydrological-related data. J. Commun. 2017, 12, 340–346.

This project has received funding from the European High-Performance Computing Joint Undertaking (JU) under grant agreement No 951732. The JU receives support from the European Union's Horizon 2020 research and innovation programme and Germany, Bulgaria, Austria, Croatia, Cyprus, the Czech Republic, Denmark, Estonia, Finland, Greece, Hungary, Ireland, Italy, Lithuania, Latvia, Poland, Portugal, Romania, Slovenia, Spain, Sweden, the United Kingdom, France, the Netherlands, Belgium, Luxembourg, Slovakia, Norway, Switzerland, Turkey, the Republic of North Macedonia, Iceland, and Montenegro. This project has received funding from the Ministry of Education, Youth and Sports of the Czech Republic (ID:MC2101).